



1 **A dataset of energy, water vapor and carbon exchange observations**
2 **in oasis-desert areas from 2012 to 2021 in a typical endorheic basin**

3

4 Shaomin Liu¹, Ziwei Xu¹, Tao Che², Xin Li³, Tongren Xu¹, Zhiguo Ren²,
5 Yang Zhang², Junlei Tan², Lisheng Song⁴, Ji Zhou⁵, Zhongli Zhu¹, Xiaofan
6 Yang¹, Rui Liu⁶, Yanfei Ma⁷

7 *Correspondence to:* Shaomin Liu (smliu@bnu.edu.cn)

8

9 ¹State Key Laboratory of Earth Surface Processes and Resource Ecology, Faculty of Geographical
10 Science, Beijing Normal University, Beijing 100875, China

11 ²Northwest Institute of Eco-Environment and Resources, Chinese Academy of Sciences, Lanzhou
12 730000, China

13 ³National Tibetan Plateau Data Center, State Key Laboratory of Tibetan Plateau Earth System and
14 Resources Environment, Institute of Tibetan Plateau Research, Chinese Academy of Sciences,
15 Beijing 100101, China

16 ⁴Key Laboratory of Earth Surface Processes and Regional Response in the Yangtze-Huaihe River
17 Basin, School of Geography and Tourism, Anhui Normal University, Wuhu 241000, China;

18 ⁵School of Resources and Environment, University of Electronic Science and Technology of China,
19 Chengdu 611731, China

20 ⁶Institute of Urban Study, School of Environmental and Geographical Sciences (SEGS), Shanghai
21 Normal University, Shanghai 200234, China

22 ⁷Hebei Technology Innovation Centre for Remote Sensing Identification of Environmental Change,
23 Hebei Key Laboratory of Environmental Change and Ecological Construction, School of
24 Geographical Sciences, Hebei Normal University, Shijiazhuang 050024, China

25

26

27

28



29 **Abstract:**

30 Oases and deserts generally act as a landscape matrix and mosaic in arid/semiarid
31 regions. The significant difference of thermal and dynamic characteristics between
32 oasis and desert surface will result in oasis-desert interaction. That is, the interaction
33 between oasis and desert system through the exchange of momentum, energy, water
34 and carbon, which can lead to a series of microclimate effects that affect the structure
35 of the atmospheric boundary layer, changes of carbon sources/sinks in oasis and the
36 local ecological environment. Therefore, studying water, heat and carbon exchange is
37 significant for achieving the goals of carbon peaking and carbon neutrality in oasis-
38 desert areas and supporting the ecological security and sustainable development of
39 oases. To monitor energy, water vapor and carbon exchange between the land surface
40 and atmosphere, a land surface process integrated observatory was established in the
41 oasis-desert area in the middle and lower reaches of the Heihe River Basin, the 2nd
42 largest endorheic basin in China. In this study, we present a suite of observational
43 datasets in artificial and natural oases-desert systems, which consist of long-term energy,
44 water vapor, carbon/methane fluxes, and auxiliary data involving hydrometeorology,
45 vegetation and soil parameters from 2012 to 2021. Half-hourly turbulent flux data were
46 acquired by an eddy covariance system and scintillometer. The hydrometeorological
47 data, including radiation, soil heat flux and soil temperature profile, gradient of air
48 temperature/humidity and wind speed/direction, air pressure, precipitation and soil
49 moisture profiles, were observed from automatic weather stations with a 10-minute
50 average period as well as the groundwater table data. Moreover, vegetation and soil



51 parameters were also supplemented in the datasets. Careful data processing and quality
52 control are implemented during data production, including data collection, processing,
53 archiving and sharing. The current datasets can be used to explore the water-heat-carbon
54 process and its influence mechanism, calibrate and validate related remote sensing
55 products, simulate energy, water vapor and carbon exchange in oasis and desert areas,
56 and provide references and representatives for other similar artificial and natural oases
57 along the Silk Road. The datasets are available from the National Tibetan Plateau Third
58 Pole Environment.

59

60 **1. Introduction**

61 Arid and semiarid regions represent approximately 30% of the global terrestrial surface
62 area (Dregne, 1991; Scanlon et al., 2006), and dryland expansion occurs under climate
63 change, especially in developing countries (Huang et al., 2015). This proportion is much
64 higher in China, as (semi)arid regions account for approximately 47% of its terrestrial
65 surface (Zhang et al., 2016a; Mao et al., 2018). An oasis is a unique ecological
66 landscape in arid and semiarid areas, which is not only the core of its ecological
67 environment but also the foundation of its economic development, especially in western
68 China, which has been an important part of the ‘Silk Road’ since ancient times. Oases
69 with less than 10% of the total area of arid regions support more than 90% of the
70 population in the arid regions of China (Chu et al., 2005; Li et al., 2016; Zhou et al.,
71 2022). The main geomorphologic feature is a wide sandy desert or Gobi (gravel desert),
72 interspersed with many oases of different sizes and shapes in the middle and lower



73 reaches of a typical endorheic basin in Northwest China (Cheng et al., 1999). The water
74 from upstream is the link connecting these ecosystems, and the oasis is the place where
75 human beings live. The oasis areas are now 3.3 times larger than those in the early
76 1950s in the region of northwestern China (Zhang et al., 2018). The oasis-desert system
77 plays a crucial role in maintaining a stable ecological environment and agricultural
78 productivity (Zhang and Zhao, 2015). However, inland river basins in arid and semiarid
79 areas are facing the crisis of ecological environment degradation, such as the drying up
80 of rivers and lakes, the degradation of natural vegetation, the intensification of land
81 desertification and the frequent occurrence of dust storms, especially in many inland
82 river basins westward along the Silk Road, such as the Tarim River Basin (Zhao et al.,
83 2013), Aral Sea Basin (Stanev et al., 2004; Crétaux et al., 2009), and Lake Urmia Basin
84 (Stone, 2015). Therefore, it is critical to maintain the balance between the oasis and
85 desert systems to achieve the goal of sustainable oasis development.

86 The particularity of the underlying surface in the oasis-desert area, e.g., the irrigation
87 cropland, riparian forest, sandy vegetation, seasonal snow and frozen soil, makes the
88 study of land–atmosphere interactions complex and needs comprehensive consideration
89 in such heterogeneous underlying surfaces. The dynamic and thermal characteristics of
90 the underlying surface of the oasis and the desert are significantly different, and the
91 oasis and desert systems interact and influence each other through momentum, energy,
92 water vapor and carbon exchange. Thus, the oasis-desert interaction will affect the
93 structure of the atmospheric boundary layer and the local ecological environment.
94 Additionally, under the influence of weather conditions, the oasis-desert interaction



95 results in the local circulation between oasis and desert and airflows form dynamic and
96 thermal inner boundary layer within the oasis (Cheng et al., 2014). These can lead to
97 the local microclimate characteristics of the oasis-desert area (Liu et al., 2020), such as
98 the wind shield effect and cold-wet island effect of the oasis, the humidity inversion
99 effect within the surrounding desert, and oasis carbon sources/sinks. These
100 microclimate effects play an important role in the self-sustaining and development of
101 oasis systems. Understanding the basic characteristics of energy, water vapor and
102 carbon exchange in oasis-desert ecosystems is important for achieving the goals of
103 carbon peaking and carbon neutrality in the oasis-desert area and supporting ecological
104 security and sustainable development of the oasis.

105 Extensive studies have investigated energy, water vapor and carbon exchange in
106 oasis-desert areas based on field and remote sensing observations (Taha et al., 1991;
107 Potchter et al., 2008; Xue et al., 2019; Wang et al., 2019; Zhou et al., 2022) and
108 numerical simulations (Chu et al., 2005; Meng et al., 2009; Georgescu et al., 2011; Liu
109 et al., 2020). Li et al. (2016) provided a complete sketch map of oasis and desert
110 interactions based on previous studies, including the oasis cold and wet island effect,
111 oasis wind shield effect (oasis effect), and air humidity inversion effect within the
112 surrounding desert (desert effect), which are important for the stability and
113 sustainability of the oasis-desert ecosystem (Liu et al., 2020). In addition, the oasis-
114 desert areas located in semiarid regions were found to be carbon sinks by previous
115 researchers (Tagesson et al., 2016; Wang et al., 2019), which can significantly affect
116 the carbon balance of arid regions and play an increasingly important role within the



117 global carbon cycle.

118 The Heihe River Basin (HRB), the second largest endorheic basin in China, is
119 characterized by artificial oases and natural oases in the middle and lower reaches,
120 respectively. Several experiments have been conducted in these oasis-desert areas, e.g.,
121 the Heihe River Basin Field Experiment (HEIFE) from 1990 to 1992 to conduct
122 comprehensive studies of atmosphere–land surface interactions over the Zhangye oasis
123 and desert area in the middle reaches of the HRB (Wang et al., 1992), the Jinta
124 experiment from 2005 and 2008 to focus on the energy and water exchange and the
125 atmospheric boundary over the Jinta oasis and desert area in the middle reaches of the
126 HRB (Wen et al., 2012), the oasis-desert area in the middle reaches and mountainous
127 area in upper reaches of watershed allied telemetry experimental research (WATER)
128 and the subsequent HiWATER (oasis-desert area in the middle and lower reaches and
129 mountainous area in upper reaches) to be a comprehensive simultaneous satellite–
130 airborne–ground observations eco-hydrological experiment (Li et al., 2009, 2013).
131 Thereafter, a multielement, multiscale, networked, and elaborate integrated observatory
132 network was established in the oasis-desert area in the middle and lower reaches and
133 mountainous area in upper reaches of the HRB since 2007 and completed in 2013 (Liu
134 et al., 2018). A quantitative understanding of the energy, water vapor and carbon
135 exchange in oasis-desert areas is crucial for recognizing the oasis-desert interactions
136 and is significant for protecting the ecological stability and socioeconomic development
137 of oases, and long-term observations are indispensable. The observations and research
138 findings from the oasis-desert area in the HRB will serve as references and



139 representatives for other similar artificial and natural oases along the Silk Road. To
140 achieve the aforementioned objective, observations should be continuously conducted,
141 and a high-quality dataset should be obtained.

142 In this paper, the integrated observatory network of the artificial and natural oasis-
143 desert areas in the middle and lower reaches in the HRB are introduced first, and the
144 observations characterizing the energy, water vapor and carbon exchange are detailed
145 explicated, which provides a 10-year dataset. Specifically, the spatial distribution and
146 design of the observation sites are summarized in Section 2. Section 3 describes the
147 data processing and quality control procedures. In Section 4, the energy, water vapor
148 and carbon fluxes and related auxiliary parameters are introduced in detail. The data
149 availability is documented in Section 5, and the conclusions are summarized in Section
150 6. This dataset can be used for comprehensive understanding of energy, water vapor
151 and carbon exchange in oasis-desert areas, and validating simulation results and remote
152 sensing products of energy, water vapor and carbon fluxes in oasis-desert areas.

153 **2. A land surface process integrated observatory network in the oasis-desert area** 154 **of the HRB**

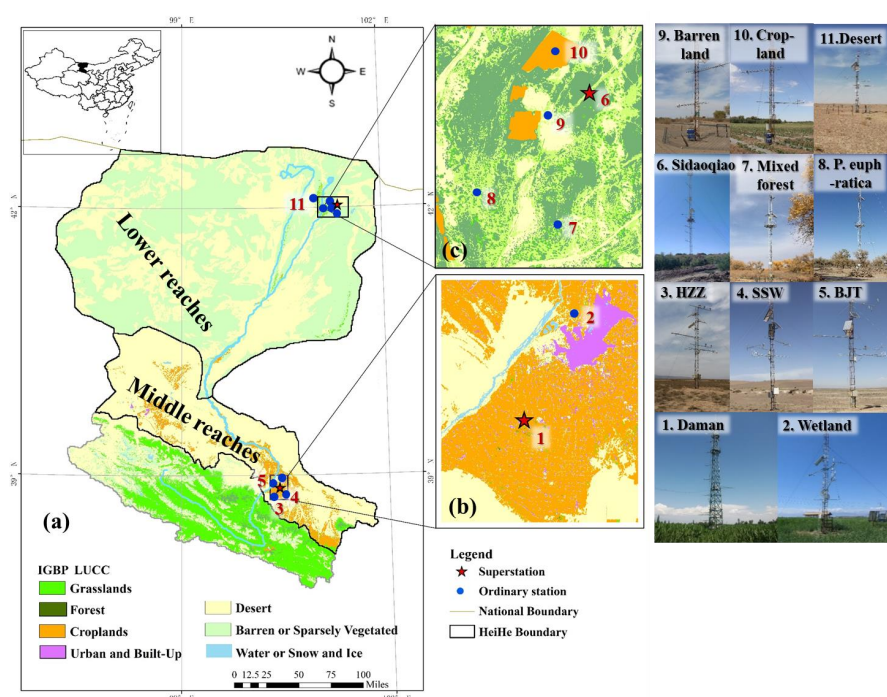
155 **2.1 Study area description**

156 The study areas are the middle and lower reaches of the HRB, which are located in
157 the arid regions of western China, provided by water from the typical cryosphere of the
158 upper reaches. The middle reaches, typical of the artificial oasis-desert system in
159 Zhangye City, the largest oasis in the Hexi Corridor, cover an area of 29,717 km² with



160 an oasis area of 5,560 km², while the lower reaches in Ejina Banner have a natural oasis-
 161 desert system covering an area of 85,678 km² with an oasis area of 1,130 km² (Fig. 1).
 162 Among the oases, agricultural oases can be traced to the history of more than 2000 years.
 163 The annual average air temperature was 7.29 °C and 9.75 °C, and the annual
 164 accumulated precipitation was 184.83 mm and 37.31 mm (1979-2018) in the middle
 165 and lower reaches, respectively.

166 Eleven land surface fluxes and meteorological stations have been established in these
 167 regions since 2012 with two superstations and eleven ordinary stations (Table 1),
 168 specifically two oasis stations and three desert stations in the middle reaches and five
 169 oasis stations and one desert station in the lower reaches.



170
 171 Fig. 1. The middle and lower reach observation systems in the HRB. (a: Heihe River
 172 basin; b: Stations in the Zhangye artificial oasis-desert area in the middle reaches; c:



173 Stations in the Ejina natural oasis area in the lower reaches)

174 Table 1. Station information in the middle and lower reaches of the HRB

ID	Name	Longitude (°, E)	Latitude (°, N)	Elevation (m)	Land Cover	Duration	Location
1	Daman	100.37	38.86	1556	Maize	May 2012- present	Oasis in midstream, superstation
2	Zhangye Wetland	100.45	38.98	1460	Wetland mainly reed	June 2012- present	Oasis in midstream, ordinary station
3	Huazhaizi Desert Steppe Shenshawo	100.32	38.77	1731	<i>Kalidium foliatum</i>	June 2012- present	Desert in midstream, ordinary station
4	Sandy Desert	100.49	38.79	1594	Sandy	June 2012- Apr.2015	Desert in midstream, ordinary station
5	Bajitan Gobi	100.30	38.92	1562	Reaumuria	May 2012- Apr.2015	Desert in midstream, ordinary station
6	Sidaoqiao	101.14	42.00	873	<i>Tamarix</i>	July 2013- present	Oasis in downstream, superstation
7	Mixed Forest	101.13	41.99	874	<i>Populus euphratica and Tamarix</i>	July 2013- present	Oasis in downstream, ordinary station
8	Populus euphratica	101.12	41.99	876	<i>Populus euphratica</i>	July 2013- Apr.2016	Oasis in downstream, ordinary station
9	Barren Land	101.13	42.00	875	Bare land	July 2013- Mar.2016	Oasis in downstream, ordinary station
10	Cropland	101.13	42.00	875	Melon	July 2013- Nov.2015	Oasis in downstream, ordinary station
11	Desert	100.99	42.11	1054	Reaumuria	Apr.2015- present	Desert in downstream, ordinary station

175 **2.2 Observation systems**

176 **2.2.1 Artificial oasis and desert areas in the middle reaches**

177 The middle reaches are located in the Zhangye oasis in Zhangye City of Gansu
 178 Province, and the primary underlying surfaces include cropland (maize), shelterbelt,
 179 orchard, residential area and wetland (reed) in the oasis and sandy desert, desert steppe



180 (*Kalidium foliatum*), and the Gobi Desert (Reaumuria) in the surrounding desert. Five
181 stations (one superstation and four ordinary stations) were established in these surfaces,
182 which are representative of the main underlying surface types within the oasis-desert
183 area in the middle reaches of the HRB.

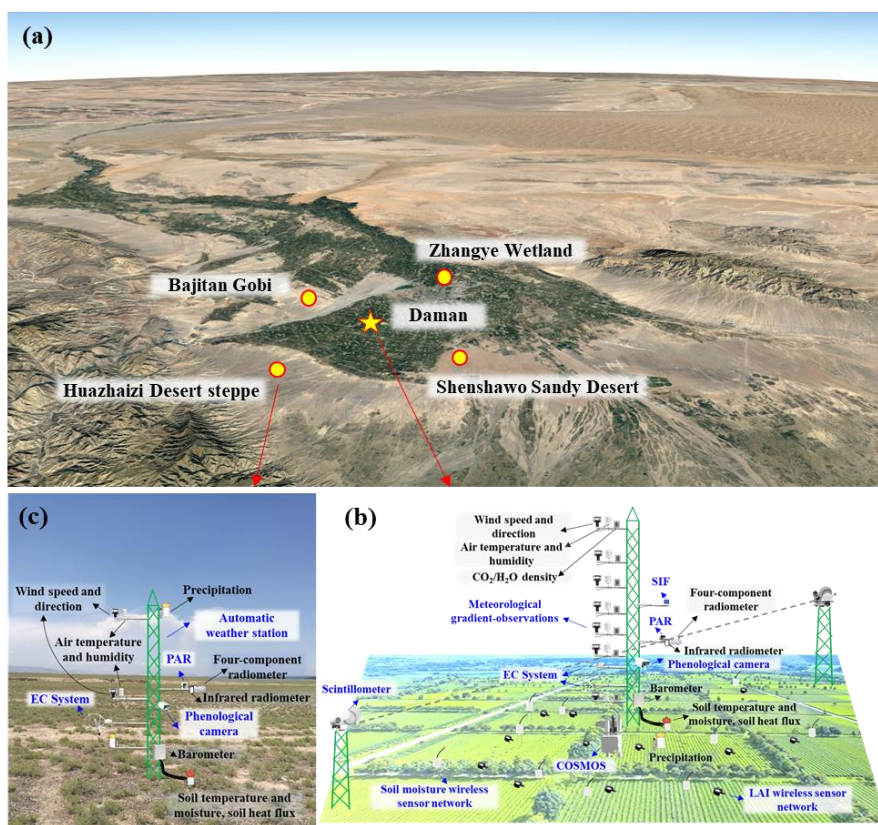
184 There is one superstation (maize and shelterbelt) and one ordinary station (wetland
185 and reed) in the Zhangye oasis surrounding three ordinary stations in the desert located
186 in the middle reaches of the HRB (Fig. 2a). The superstation includes a multiscale
187 observation system for energy, water vapor and carbon fluxes (lysimeter-EC system-
188 scintillometer for meter-hundred-kilometer observation scale) and soil moisture
189 measurements (*in situ* soil moisture profile-cosmic ray probe-soil moisture wireless
190 sensor network for meter-hundred-kilometer observation scale), and it includes a
191 hydrometeorological gradient observation system to monitor the profile (7 layers) of
192 wind speed/direction, air temperature/humidity and carbon dioxide and water vapor
193 concentration, one layer four-component radiation, air pressure, precipitation, and
194 infrared temperature (2 repetitions), 9/8 layers' soil temperature/moisture profile, soil
195 heat flux (3 plates with two buried under the bare soil between two corn plants and one
196 buried under the corn plants), etc. The EC and hydrometeorological gradient
197 observation system were installed on a 40 m tower. Optical and microwave
198 scintillometers were installed on both sides of the 40 m tower apart from 1854 m. There
199 were also observations of vegetation parameters in the 40 m tower, including a visible
200 and near infrared phenological camera to monitor the vegetation index and crop growth
201 curve, two photosynthetically active radiation (PAR) sensors to monitor PAR, a



202 vegetation chlorophyll fluorescence observation system to monitor sun-induced
203 chlorophyll fluorescence (SIF), and an LAI wireless sensor network (28 nodes) to
204 monitor multipoint LAI in the source area of the scintillometer (Fig. 2b, Fig. 4a).

205 The ordinary stations are comprised of an EC system, an automatic weather station
206 (AWS) and a visible and near infrared phenological camera. The observation elements
207 of the AWS include two layers' air temperature/humidity and wind speed/direction, one
208 layer's four-component radiation, air pressure, and infrared temperature (2 repetitions),
209 two layers' precipitation, 8/7 layers' soil temperature/moisture, soil heat flux (3 plates),
210 etc. (Fig. 2c).

211 The sonic anemometers of the ECs were installed at a height of approximately 3-7 m
212 above the canopy to capture the sensible heat, latent heat, carbon dioxide and methane
213 (in wetland) fluxes, etc. The sonic anemometers of all the ECs were aimed toward the
214 north. Soil parameters, such as soil texture, porosity, bulk density, saturated hydraulic
215 conductivity, and soil organic matter content, etc. were investigated at each station in
216 2012 and 2020. Detailed information can be found in Table 2.



217

218 Fig. 2. Sketch map of the artificial oasis and desert area in the middle reaches (a:
219 artificial oasis and desert area (from © Google Earth); b: Daman superstation; c:
220 Huazhaizi ordinary station)

221 2.2.2 Natural oasis and desert areas in the lower reaches

222 The Ejin Banner oasis is located in the lower reaches of the HRB and belongs to
223 Inner Mongolia and part of Jiuquan city of Gansu Province, which is surrounded by
224 widespread desert. The main underlying surfaces were Reaumuria and terminal lake in
225 desert, riparian forest, cropland, barren land and residential area in the oasis in the lower
226 reaches. There were six stations (one superstation and five ordinary stations) in the



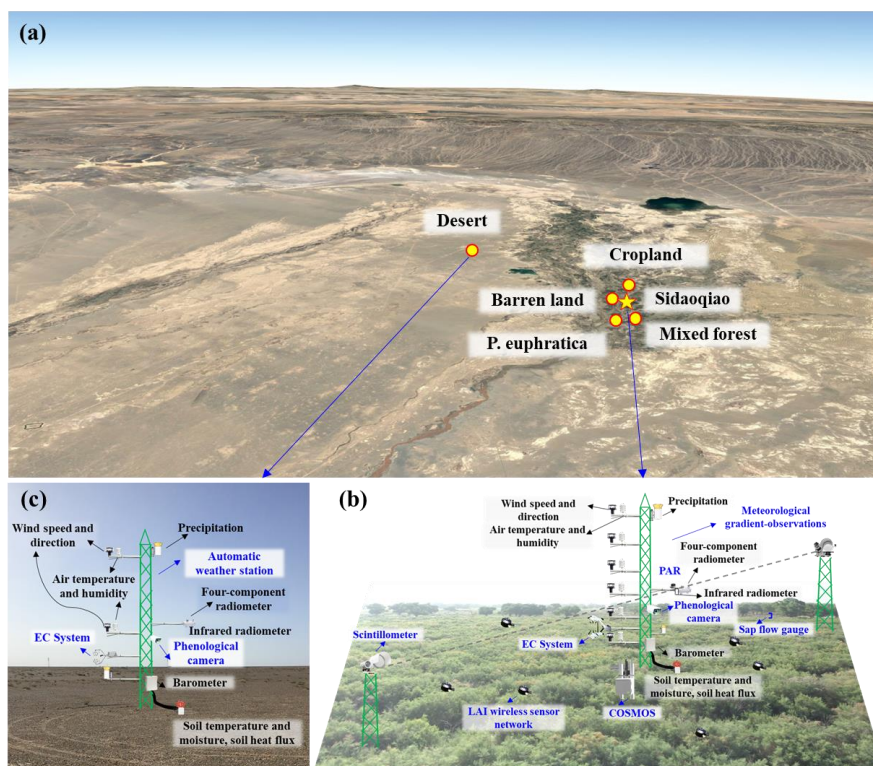
227 lower reaches, which are located in these land covers, including *Populus euphratica*,
228 *Tamarix chinensis*, cropland, barren land, and desert.

229 In the oasis-desert area of the lower reaches, there is one superstation and four
230 ordinary stations in the oasis and one ordinary station in the desert (Fig. 3a). The
231 superstations include a multiscale observation system for energy, water vapor and
232 carbon fluxes (sap flow gauge-EC-large aperture scintillometer for meter-hundred-
233 kilometer observation scale) and soil moisture measurements (*in situ* soil moisture
234 profile and cosmic ray probe for meter and hundred meter observation scale), a
235 hydrometeorological gradient observation system to monitor the profile (6 layers) of
236 wind speed/direction, air temperature/humidity, one layer four-component radiation, air
237 pressure, and infrared temperature (2 repetitions), two layers of precipitation, 10/9
238 layers soil temperature/moisture profile, soil heat flux (with two buried under the bare
239 soil and one buried under the *Tamarix* plants), etc. The EC and hydrometeorological
240 gradient observation system were installed on a 28 m tower. Two groups of large
241 aperture scintillometers were installed on both sides of the 28 m tower apart from 2350
242 m. The vegetation parameter observations included PAR and the phenological camera
243 to monitor the vegetation index and crop growth curve installed in the 28 m tower and
244 LAI wireless sensor network (11 nodes in the source area of the scintillometer) (Fig. 3b,
245 Fig. 4b). The ordinary stations are comprised of an EC system, an AWS and a visible
246 and near infrared phenological camera. (Fig. 3c).

247 Additionally, thermal infrared radiometers and imagers were installed at the Mixed
248 Forest and Sidaoqiao stations to measure different component temperatures, i.e., the



249 brightness temperature of different land cover types under different illumination
 250 conditions (Li et al., 2019). The soil parameters and groundwater table were observed
 251 around the stations. Detailed information can be found in Table 2.



252
 253 Fig. 3 Sketch map of the natural oasis and desert areas in the lower reaches (a: natural
 254 oasis and desert area (from © Google Earth); b: Sidaoqiao superstation; c: desert ordinary
 255 station)

256 Table 2 Observation variables and sensor configurations of surface flux,
 257 hydrometeorology, vegetation and soil parameters

Observations	Sensor	Manufactory	Height/depth (m)	Sites
<i>Surface flux observations:</i>				
Sensible heat, latent heat, carbon dioxide, methane flux	CSAT3&Gill, Li7500&Li7500 A&Li7500DS& EC155&Li7700	Campbell and LiCor, USA	3~7 m above the canopy	All stations (methane observation only in wetland, closed path EC at Daman and Desert,



		CPEC310 stations)		
Sensible and latent heat flux	BLS900 and MWSC-160	Scintec and RPG, Germany	23.92	Daman
	BLS900	Germany	25.5	Sidaoqiao
Sap flow	TDP 30	Rainroot, China	1.5	Mixed forest
<i>Hydrometeorological observations:</i>				
Pressure	PTB110	Vaisala, Finland	--	Bajitan, Shenshawo
	AV-410BP	Avalon, USA	--	Mixed Forest
	PTB210	Vaisala, Finland	--	Huazhaizi
	CS100	Campbell, USA	--	Daman, Wetland, Sidaoqiao, Desert
Precipitation	TE525MM	Texas Electronics, USA	--	Daman, Wetland, Huazhaizi, Bajitan, Shenshawo, Sidaoqiao, Desert
	52203	RM Young, USA	--	Mixed Forest
Wind speed/direction	Windsonic	Gill, UK	3,5,10,15,20,30,40	Daman, Sidaoqiao
			5,7,10,15,20,28	
			5,10	Wetland, Huazhaizi, Mixed forest
	010C/020C	Met One	5,10	Wetland, Desert
Air temperature/humidity	03001	RM Young, USA	10	Bajitan, Shenshawo
			28	Populus euphratica
	HMP45D	Vaisala, Finland	28	Mixed Forest
	HC2S3	Vaisala, Finland	5,7,10,15,20,28	Sidaoqiao
HMP45AC	Vaisala, Finland	5,10	Bajitan, Huazhaizi, Shenshawo, Wetland, Desert	
		28	Populus euphratica	
Four-component	AV-14TH	Avalon	3,5,10,15,20,30,40	Daman
			CNR4	Kipp&Zonen, Netherland



radiation	CNR1	Kipp&Zonen, Netherland	6	Wetland,Huazhaizi,Bajitan,Shenshawo,Desert,Barren land, Cropland
			22	Populus euphratica
	PSP&PIR	Eppley, USA	12	Daman
			12	Daman
			10	Sidaoqiao
Infrared temperature	SI-111	Apogee, USA	22	Populus euphratica, Mixed Forest
			6	Wetland,Huazhaizi,Bajitan,Shenshawo,Desert,Barren land, Cropland
	109ss-L	Campbell, USA	0,-0.02,-0.04,-0.1,-0.2,-0.4,-0.8,-1.2,-1.6,-2.0	Sidaoqiao,
			0,-0.02,-0.04,-0.1,-0.2,-0.4,-0.6,-1.0	Desert Wetland
			0,-0.02,-0.04,-0.1,-0.2,-0.4,-0.6,-0.8,-1.2,-1.6	Daman
Soil temperature profile	AV-10T	Avalon, USA	0,-0.02,-0.04,-0.1,-0.2,-0.4,-0.6,-1.0	Bajitan, Huazhaizi
			0,-0.02,-0.04,-0.1,-0.2,-0.4	Wetland
			0,-0.02,-0.04,-0.1,-0.2,-0.4,-0.6,-1.0,-1.6,-2.0,-2.4	Mixed forest
	109	Campbell, USA	0,-0.02,-0.04,-0.1,-0.2,-0.4,-0.6,-1.0	Shenshawo
			0,-0.02,-0.04	Barren land, Cropland, Populus euphratica
	ECH ₂ O-5	Decagon Devices, USA	-0.02,-0.04,-0.1,-0.2,-0.4,-0.6,-1.0	Bajitan
Soil moisture profile	CS616	Campbell, USA	-0.02,-0.04,-0.1,-0.2,-0.4,-0.6,-0.8,-1.2,-1.6	Shenshawo, Desert
				Daman
	ML2X	Delta-T, UK	-0.02,-0.04,-0.1,-0.2,-0.4,-0.8,-1.2,-1.6,-2.0	Sidaoqiao
			-0.02,-0.04,-0.1,-0.2,-0.4,-0.6,-1.0,-1.6,-2.0,-	Mixed Forest



			2.4	
			-0.02, -0.04	Barren land, Populus euphratica, Cropland
	ML3	Delta-T, UK	-0.02,-0.04,-0.1,-0.2,-0.4,-0.6,-1.0	Desert, Huazhaizi
Soil heat flux	HFP01	Hukseflux, Netherland		Wetland,Huazhaizi, Bajitan,Shenshawo,Desert,Barren land, Cropland
	HFT3	Campbell, USA	-0.06	Bajitan, Populus euphratica, Mixed forest
	HFP01SC	Hukseflux, Netherland		Daman, Sidaoqiao
Averaged temperature	TCAV	Campbell, USA	-0.02, -0.04	Daman, Sidaoqiao
CO ₂ /H ₂ O profile	AP200	Campbell, USA	3,5,10,15,20,30,40	Daman
Groundwater Table	U20	Onset, USA	-2~-3m	Sidaoqiao, Mixed forest, Populus euphratica, Cropland, Desert
<i>Vegetation parameter observations:</i>				
Vegetation phenology	Phenological camera	XST-PhotoNet, China	above the canopy	All sites
LAI	XST- LAINet	Beijing StarViewer Science and Technology Ltd., China	Below the canopy	28 nodes around Daman, 6 nodes around Sidaoqiao, 5 nodes around Mixed forest
photosynthetically active radiation	PQS-1	Kipp&Zonen, Netherland	0.5, 12	Daman
			10	Sidaoqiao
			22	Mixed forest, Populus euphratica
			6	Wetland, Cropland
Sun-induced chlorophyll fluorescence	AutoSIF-1	Beijing Bergsun Spectral Technology Co. Ltd, China	34	Daman

Soil parameters: soil sampling and laboratory testing in 2012 and 2020

258

259 3. Data processing and quality control

260 The data processing and quality control procedure can be divided into data collection,



261 data processing and data archiving and sharing (Fig. 4).

262 In the data collection step, the comparison and calibration of instruments are
263 prerequisites to ensure the quality of the observation data. The instrument comparison
264 experiments were specifically arranged under the Gobi Desert in 2012 in the middle
265 reaches (Xu et al., 2013) and shrub in 2013 in the lower reaches (Li et al., 2018) to
266 ensure the consistency and comparability of the instruments. In addition, the
267 instruments with multiple layers were compared at the same height before installation,
268 the soil moisture probes were also compared under dry and wet conditions, and the
269 multitype rain gauges were compared in the same field. The infrared gas analyzer of all
270 the EC systems was calibrated at the beginning and end of the vegetation-growing
271 season every year. To ensure the data quality, a routine maintenance procedure is
272 formulated and strictly followed, including daily (checking the real-time data through
273 remote monitoring and data management system for field observatory network v1.0),
274 10 days (checking the time series plot providing by the system), monthly (routine
275 inspection in every station), and annually (data processing and release) (Liu et al., 2018).
276 The Heihe watershed internet of things observation system was developed to complete
277 the above maintenance procedure, which included remote receiving and storing the filed
278 data, browsing and processing real-time data, monitoring the instrument status and early
279 warning the abnormal conditions, etc.

280 During the data processing step, a processing scheme was formulated for each type
281 of instrument. For the EC system, the data were processed from the raw 10 Hz turbulent
282 data, including spike detection, sonic temperature correction, coordinate rotation,

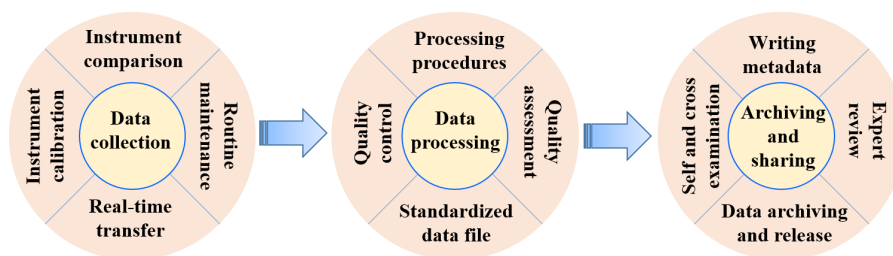


283 frequency response correction, and WPL (Webb-Pearman-Leuning) correction. (Liu et
284 al., 2016; Wu et al., 2023). Additionally, the 30-min flux data series were identified as
285 quality flags according to the stationarity test and integral turbulence characteristics test.
286 A final quality flag (1~9) was assigned to each specific turbulent flux value, indicating
287 good quality (1~3), suitability for general use (4~6), poor but better than gap filling data
288 (7~8), and discarded data (9). The data processing steps from scintillometer
289 measurements to surface fluxes are as follows: raw data to light intensity variance, light
290 intensity variance to the structure parameter of the refractive index of air (C_n^2), C_n^2 to
291 meteorological data, and finally obtaining surface fluxes combining the meteorological
292 data. Four steps are taken to ensure the quality of scintillometer data (Liu et al. 2011;
293 Zheng et al., 2023): (i) excluding data for C_n^2 beyond the saturation criterion; (ii)
294 excluding data obtained during periods of precipitation; (iii) excluding data when the
295 demodulated signal is small; and (iv) excluding data when the sensor is malfunctioning.
296 The steps of the meteorological gradient observation system and AWS data processing
297 and quality control were twofold: (1) all the AWS data were averaged over an interval
298 of 10 min for a total of 144 records per day. The missing data were denoted by -6999;
299 (2) the unphysical data were rejected, and the gaps were denoted by -6999. The surface
300 soil heat flux was calculated using the 'PlateCal' approach (Liebethal et al., 2005), and
301 the final surface soil heat flux was the weighted vegetation fraction combined with the
302 soil temperature and moisture measured above the heat plates. The vegetation growth
303 curve and vegetation index can be obtained from visible and near infrared bands
304 measured by phenological cameras. The key phenological parameters are determined



305 according to growth curve fitting, such as the growth season start date, peak, and growth
306 season end. The leaf area index (LAI) data were obtained from the LAI_{Net} sensor,
307 which can continuously measure the multipoint total solar radiation above the canopy
308 and the transmitted radiation below the canopy, and the LAI was calculated based on
309 multiangle transmittance data (Qu et al., 2014). Then, all the data are processed into a
310 standardized file for sharing.

311 During the archiving and sharing step, the metadata were written for each data point,
312 including the site description, processing step, header description, and other notes. (Li
313 et al., 2017a). Before data are released, self-examination, crosschecks and expert review
314 are required to ensure data quality. Finally, the data were archived and shared online.



315

316

Fig. 4 Flowchart of data processing and quality control

317 4. Data description

318 4.1 Energy, water vapor and carbon fluxes data

319 The EC systems were used to measure surface flux at all sites, namely, 5 stations (2
320 in oasis, 3 in desert) in the middle reaches and 6 stations (5 in oasis, 1 in desert) in the
321 lower reaches. The turbulent flux data were recorded by the open path or closed path
322 EC systems and processed carefully. In addition to the surface flux of sensible, latent
323 and carbon dioxide, the methane flux was also observed at the wetland site in the middle
324 reaches (Table 2). The multiyear seasonal variations in sensible heat, latent heat, carbon



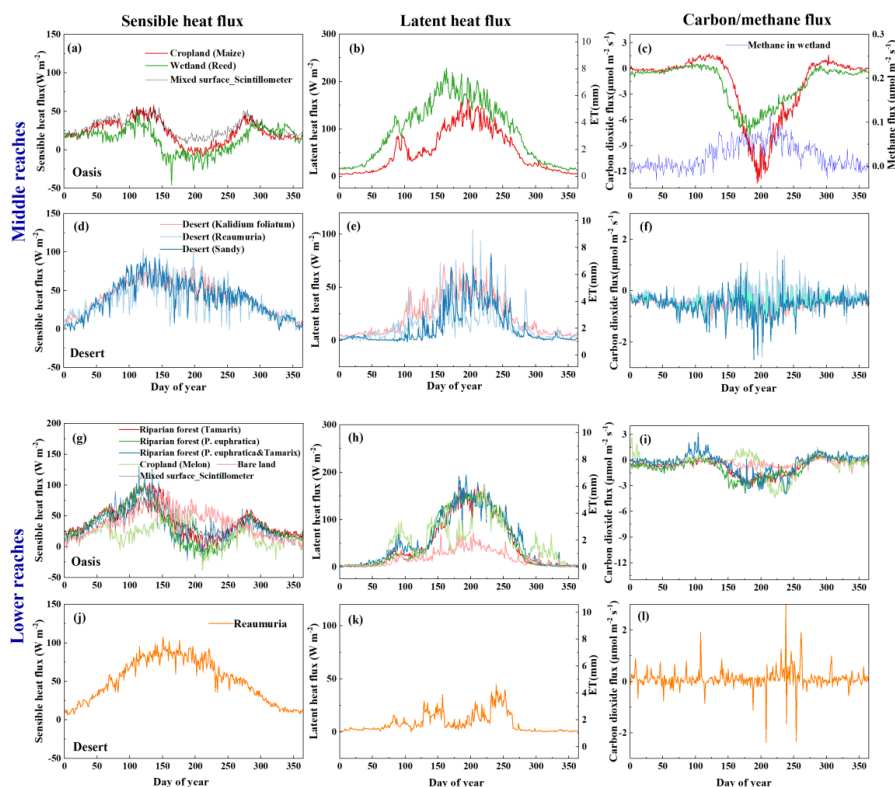
325 dioxide and methane fluxes are shown in Figure 5. Generally, the latent heat fluxes in
326 oases are obviously higher than those in deserts, especially in the lower reaches. The
327 latent heat fluxes exhibited a single peak during one year, with a peak value of
328 approximately 200 W m^{-2} in the oasis area; however, they significantly fluctuated due
329 to irrigation (normally 4 times in cropland of the midstream region, 2 times in riparian
330 forest and melon of the downstream region) or precipitation. In the middle reaches, the
331 latent heat flux in the wetland showed the largest values, which were more than 200 W
332 m^{-2} in the crop growing season, and it also presented relatively large values in the
333 midstream piedmont desert region with dense *Kalidium foliatum* cover (peak value
334 greater than 50 W m^{-2}). In the lower reaches, the latent heat flux showed consistent
335 variations in the riparian forest with a peak value of approximately 150 W m^{-2} during
336 the crop growing season; however, it showed large fluctuations in the melon surface
337 during growth due to frequent irrigation (approximately 7~8 times), and the bare land
338 in the oasis and desert had a small latent heat flux.

339 The seasonal variations in sensible heat flux were totally different in the oasis and
340 desert systems. The sensible heat flux showed two peaks in the oasis in both the middle
341 and lower reaches except for the bare land, namely, reaching maximum values at the
342 end of April and September, and it showed minimum values in mid-August (-25 W m^{-2}),
343 corresponding to large values of latent heat flux in the oasis that were even greater
344 than net radiation. This phenomenon was also found by previous researchers (Liu et al.,
345 2011) and was called the ‘oasis effect’. In the desert area, the sensible heat flux appeared
346 as a single peak in spring and decreased gradually since then. The variation in sensible
347 heat flux in bare land of the natural oasis in the lower reaches is similar to that in the
348 desert area.

349 In the oasis, the carbon dioxide (CO_2) flux showed obvious ‘U’ variations, especially



350 in the middle reaches. The crop absorbed carbon dioxide (carbon sink) in the crop-
351 growing season, and a negative value of approximately $-14 \mu\text{mol m}^{-2} \text{s}^{-1}$ was observed
352 in the maize surfaces. The magnitude of the methane (CH_4) flux was lower than the
353 CO_2 flux and was in the range of approximately $0\sim 0.1 \mu\text{mol m}^{-2} \text{s}^{-1}$ in the wetland. The
354 CH_4 flux in the non-growing season was the lowest and increased rapidly in April.
355 Although the magnitude of the CH_4 flux was lower than the CO_2 flux, the contribution
356 of methane emissions to global warming was as important as CO_2 contributions on a
357 long time scale (Hommeltenberg et al., 2014; Zhang et al., 2016b), especially focusing
358 on CH_4 flux measurements in wetlands (Zhang et al., 2022). The variations in CO_2 flux
359 in the riparian forest were relatively small, with values of approximately $-0.4 \mu\text{mol m}^{-2}$
360 s^{-1} in the plant growing season. There was little carbon sequestration in the desert area
361 due to little or sparse vegetation, and the CO_2 flux in the desert area was very small,
362 fluctuating around zero during the years.



363

364 Fig. 5 The multiyear seasonal variations in sensible, latent heat, carbon dioxide and
 365 methane fluxes in the oasis-desert area (sensible heat flux—left, latent sensible heat
 366 flux—middle, carbon dioxide and methane flux—right, 2012–2021)

367 **4.2 Hydrometeorological data**

368 The hydrometeorological data were obtained from 13 AWSs, with six in the middle
 369 reaches (Fig. 2) and seven in the lower reaches (Fig. 3) of the HRB. All the AWSs
 370 recorded four-component radiations (short/long wave upward and downward radiation),
 371 soil heat flux, surface and soil temperature profiles, air temperature and humidity, wind
 372 speed and direction, air pressure, precipitation, soil moisture profiles, and groundwater



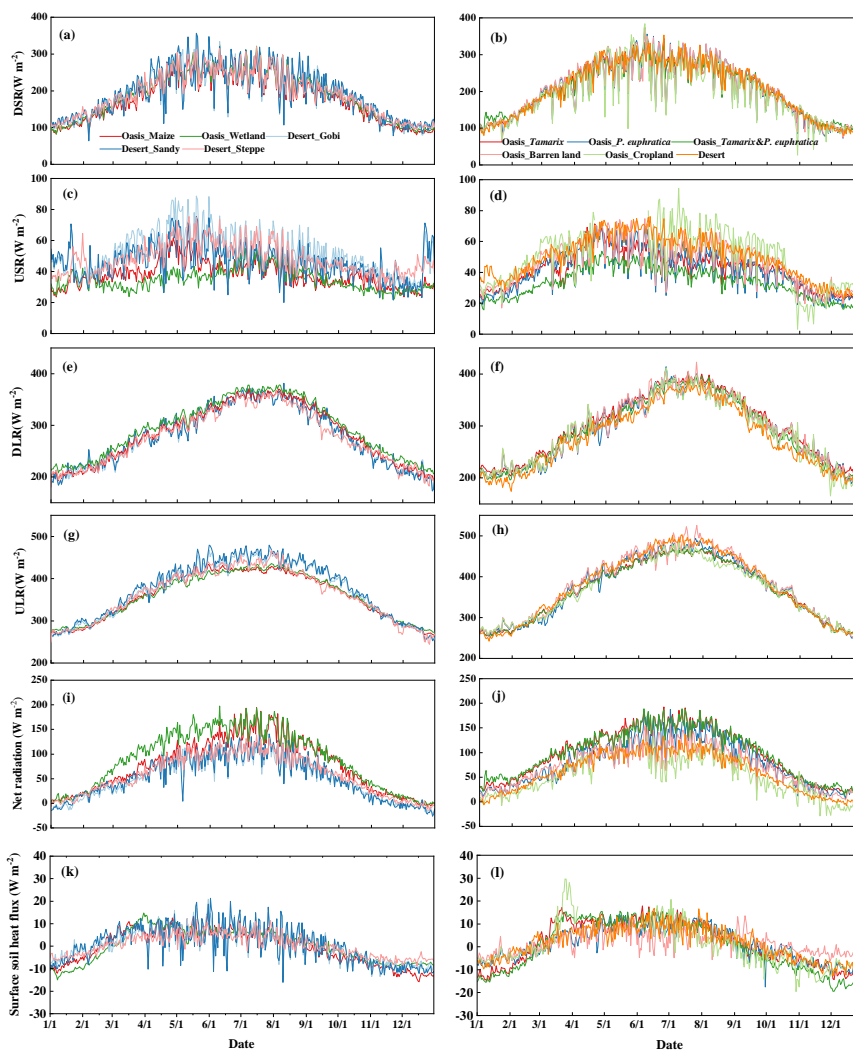
373 table, etc. (Table 2). All sensors were calibrated and intercompared before being
374 mounted. The sampling frequencies, reference heights and directions of these sensors
375 at all stations were identical to maintain consistency.

376 4.2.1 Radiation, soil heat flux, surface and soil temperature profile

377 It is important to understand the variations in radiation and surface soil heat flux in
378 oasis and desert areas, which are the surface available energy. Figure 6 shows the four
379 radiation components and soil heat flux in oasis and desert areas in the middle and lower
380 reaches in the HRB, and all the variables exhibited obvious seasonal variations with an
381 inverted ‘U’ shape. The incoming shortwave radiation was consistent with each other
382 in oasis and desert because of the short distance among the sites. Due to the higher
383 albedo in the desert, the upward shortwave radiation in the desert was larger than that
384 in the oasis (approximately larger than 30%). The incoming longwave radiation
385 originates from the atmosphere (in particular CO₂ and water vapor) and thermal
386 radiation of clouds in the lower atmosphere. The oasis presents relatively large water
387 vapor and cloudiness; thus, the incoming longwave radiation for the oasis was greater
388 than that for the desert (approximately 2%). It is to be expected that under dry
389 conditions during the daytime, the surface temperature of the desert will be significantly
390 greater than that of the well-watered oasis site. Consequently, the upward longwave
391 radiation in the desert was larger than that in the oasis (approximately 8%). The net
392 radiation, driving the turbulent fluxes of sensible heat and latent heat at the earth surface
393 and heating soil, was greater in the artificial oasis and the natural oasis than in the desert
394 at approximately 50 W m⁻². The daily mean surface soil heat fluxes varied similarly in



395 oasis and desert areas with relatively low values in the range of -20 to 20 W m^{-2} .

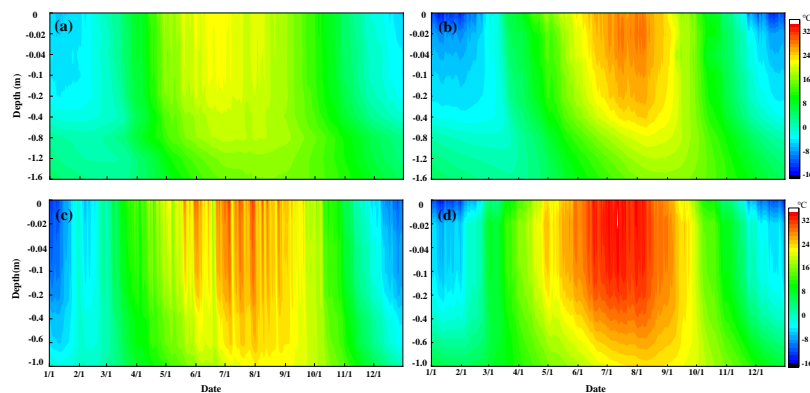


396
397 Fig. 6 Seasonal variations in multiyear average radiation components in the oasis-desert
398 system (middle reaches: a, c, e, g, i, k; lower reaches: b, d, f, h, j, l; 2012-2021 daily
399 averaged DSR: downward shortwave radiation; USR: upward shortwave radiation;
400 DLR: downward longwave radiation; ULR: upward longwave radiation)

401 The soil temperature exhibited a signal peak around the year in the range of -
402 $15^{\circ}\text{C}\sim 34^{\circ}\text{C}$, and it decreased with increasing soil depth during the plant growing season;



403 however, it exhibited an increasing trend in the winter. The shallow soil began to thaw
404 at the beginning of spring (march) and to freeze in autumn (November). The soil
405 temperature changed little with depth when it exceeded 0.8 m and 1 m in the oasis and
406 desert, respectively. The soil temperature in the desert was significantly higher by
407 approximately 10 °C during the plant growing season than that in the oasis in both the
408 middle and lower reaches. Additionally, the soil temperature in the artificial oasis-desert
409 area (middle reaches) was approximately 5 °C lower during the plant growing season
410 than that in the natural oasis-desert area (lower reaches) (Fig. 7).



411
412 Fig. 7. Seasonal variations in surface and soil temperature profiles in oasis and desert
413 areas (2012-2021) (a: oasis in middle reaches–maize; b: oasis in lower reaches–*Tamarix*;
414 c: desert in middle reaches–*Reaumuria*; d: desert in lower reaches–*Reaumuria*)

415 4.2.2 Air temperature/humidity, wind speed/direction, air pressure

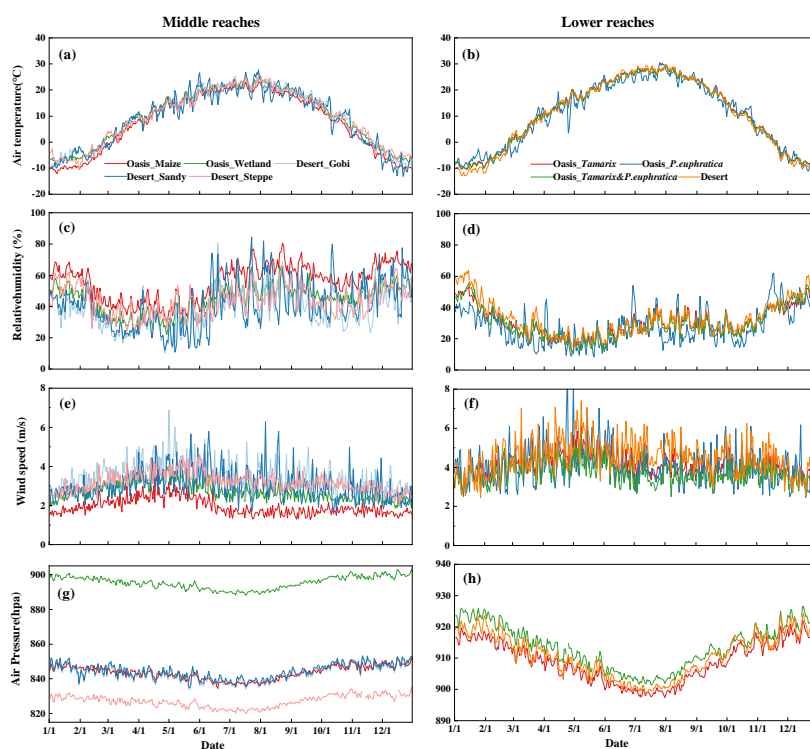
416 To show micrometeorological characteristics clearly, the comparison of daily average
417 air temperature and relative humidity (5 m except the *P. euphratica* surface with a height
418 of 28 m), wind speed (10 m) and air pressure in desert and oasis are plotted in Figure 8.
419 The seasonal variation in air temperature in the oasis and desert was similar; however,



420 the air temperature in the desert was generally higher than that in the oasis by
421 approximately 0.6 °C on average annually (approximately 0.4 °C in the plant growing
422 season). Instead, the relative humidity in the desert was lower than that in the artificial
423 oasis in the midstream region (approximately 9% and 10% in the annual and plant
424 growing seasons, respectively). The relative humidity in natural oasis and desert areas
425 are similar due to the extreme arid regions with rare precipitation, little irrigation
426 amount and small natural oasis area. Generally, the desert surface has the characteristics
427 of high temperature and lower humidity, and the oasis is a cold and wet island. In the
428 middle and lower reaches of the oasis and desert areas, the wind speed in the desert was
429 obviously larger than that in the oasis because of the wind shield effect in the oasis
430 (middle reaches: 1~3 m/s in the oasis, 2~6 m/s in the desert; lower reaches: 3~6 m/s in
431 the oasis, 3~7 m/s in the desert), and the wind speed decreased significantly when
432 passing by the windbreaks, buildings and crops, especially in the artificial oasis in the
433 middle reaches. The lower wind speed in oases is helpful to plant growth, people's
434 survival environment and the maintenance of oasis and desert ecosystems (Wang and
435 Cheng, 1999). While the seasonal variation in wind speed between desert and oasis was
436 similar, this indicated that they were controlled by the same synoptic system. The wind
437 speed in the natural oasis in the lower reaches was higher than that in the artificial oasis
438 in the middle reaches. The maximum wind speeds were observed in April in the
439 artificial and natural oases, respectively, while the minimum values were observed in
440 July. The air pressure decreased with decreasing elevation, e.g., the air pressure in the
441 middle reaches with relative high elevation was lower than that in the lower reaches, as



442 well as the discrete distribution of stations in the middle reaches with different
443 elevations (Fig. 10g and h, Table 1).

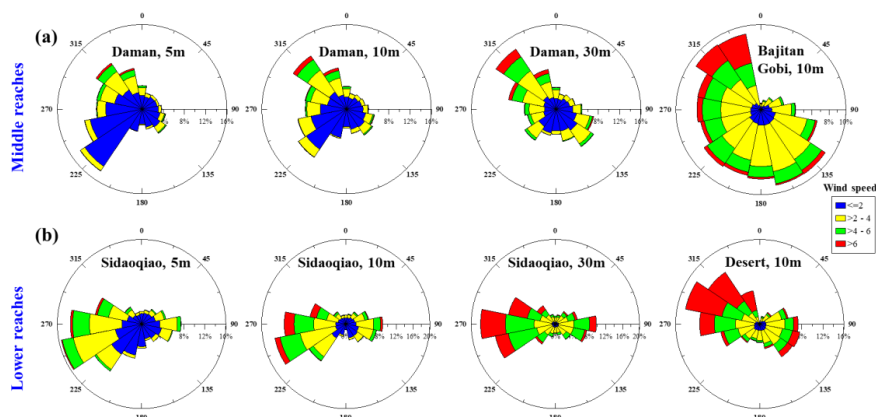


444
445 Fig. 8 Micrometeorological comparison between the oasis and desert (a, b: air
446 temperature; c, d: relative humidity; e, f: wind speed; g, h: air pressure, 2012-2021)

447 Windbreaks, buildings, crops or riparian forests drag on the wind flow inside the oasis,
448 and the wind direction is different in the oasis and desert. In the middle reaches, the
449 dominant wind directions in the desert are the northwest wind and southeast wind
450 directions, while they are northwest and southwest (10 m) in the oasis cropland;
451 however, with the increase in observation height, the influence of surface roughness on
452 wind speed/direction decreased, and the southwest wind gradually decreased, while the
453 northwest wind and southeast wind gradually increased, which is similar to the wind in



454 the desert area around the oasis (~30 m height). In the lower reaches, the wind direction
455 was similar in the oasis and desert areas, with prevailing wind directions of west and
456 east (Fig. 9).

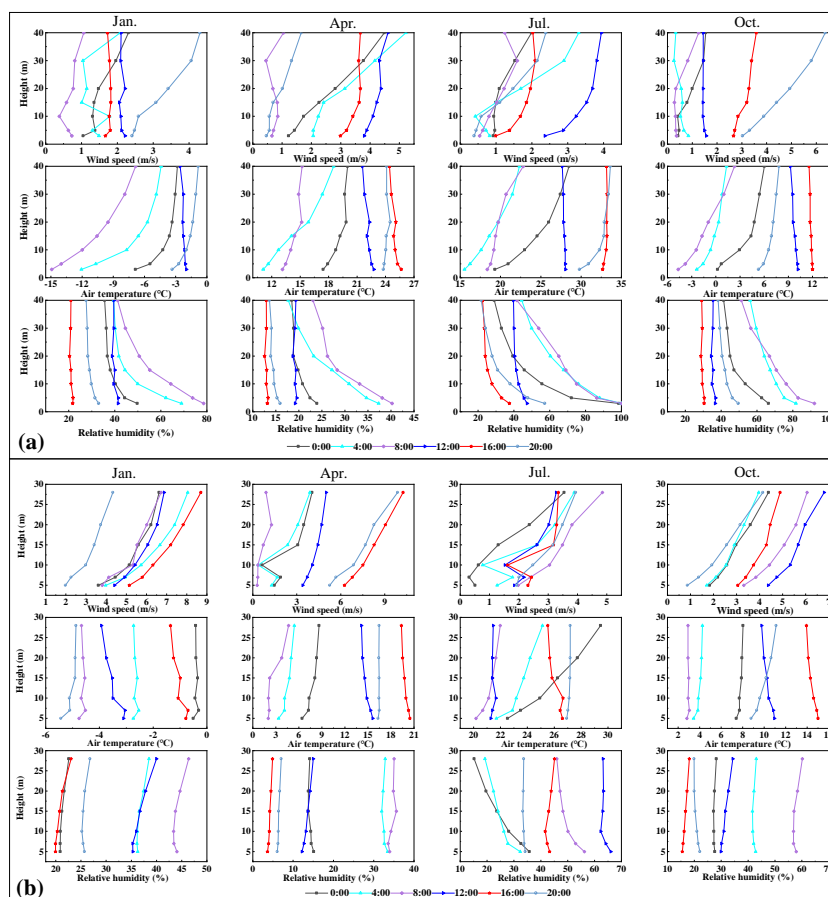


457
458 Fig. 9 Wind speed/direction in the oasis and desert area (2012-2021) (a: artificial oasis-
459 desert area in middle reaches; b: natural oasis-desert area in lower reaches; legend is
460 wind speed)

461 There are six/seven layer gradient observations of wind, air temperature and
462 humidity in superstations in artificial and natural oases. Data on typical days during
463 January, April, July and October in 2021 were selected, and the profiles of wind speed,
464 air temperature and humidity are plotted in Fig. 10. The wind speed generally increased
465 with the observation height, especially in the natural oasis. The air temperature showed
466 inversion at night during atmospheric stable stratification and changed little even below
467 10 m in the afternoon in July at both artificial and natural oases, which may be caused
468 by oasis-desert interactions. The relative humidity was low during the daytime and
469 maintained high values at night, decreasing with the observation height, especially



470 below 10 m.



471

472 Fig. 10 The profile of wind speed, air temperature and relative humidity in typical days
473 of January 14, April 14, July 14 and October 14 in 2021 (a: artificial oasis in middle
474 reaches; b: natural oasis in lower reaches)

475 4.2.3 Precipitation, soil moisture and groundwater table

476 Figure 11 shows the variations in precipitation, soil moisture profiles and
477 groundwater table (lower reaches) in typical oasis and desert ecosystems. Precipitation
478 in the middle reaches was higher than that in the lower reaches, and it was higher in the

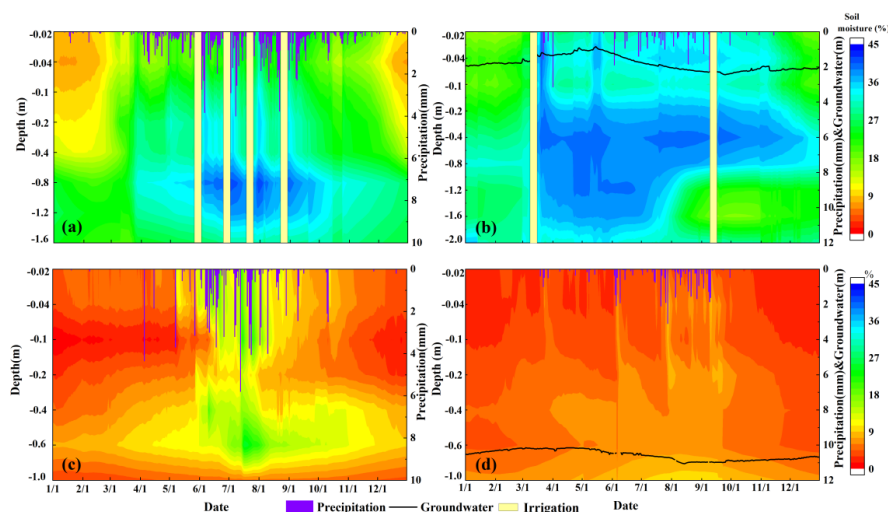


479 oasis than in the desert. The soil moisture in the oasis was significantly higher than that
480 in the desert, and it was especially small in the desert of the lower reaches. The soil
481 moisture exhibited an increasing trend with increasing soil depth, especially in the oasis.
482 The soil moisture was higher at depths of 0.8-1 m in the artificial oasis in the middle
483 reaches and at depths of 0.4-0.8 m in the natural oasis in the lower reaches. Soil crust
484 appeared in the lower reaches due to soil salinization, and it may prevent the loss of soil
485 moisture. When a precipitation event occurred, the soil moisture in the desert increased
486 accordingly; however, there were no clear variations in the oasis. There were usually
487 four irrigation events in the artificial oasis in the middle reaches, and the soil moisture
488 increased clearly accordingly, while some occasional peaks in soil moisture were due
489 to relative heavy precipitation (Fig. 11a). In the lower reaches, two irrigation events
490 (usually in March and September) generally occurred in riparian forests in natural oases.
491 The shallow soil moisture showed large values in March when irrigation occurred and
492 decreased in the plant growing season with a slight increase in September. Another
493 phenomenon is that the precipitation in the artificial oasis was larger than that in the
494 desert, although the sites were not far away from each other (e.g., 103.1 mm at the
495 Daman superstation and 75.4 mm at the Gobi station). From the analysis, the soil
496 moisture in the desert was strongly dependent on precipitation (Fig. 11c, d), while it
497 maintained high values in the plant growth season relying on irrigation in the oasis.

498 In the lower reaches, five systems for groundwater table measurement have operated
499 since June 2014 in the oasis, near the Sidaoqiao, Mixed Forest, *Populus euphratica*,
500 Cropland, and Barren Land stations. The groundwater table was approximately 1–3 m



501 under the ground, and the groundwater table level declined from a depth of
502 approximately 1 m to 3 m in the growing season to supply the riparian forest growth
503 (Fig. 11b). Additionally, one groundwater table measurement system was installed near
504 the desert station in 2018. The depth of the groundwater table level was approximately
505 10-11 m in the desert and showed no significant variation over the years (Fig. 11d).



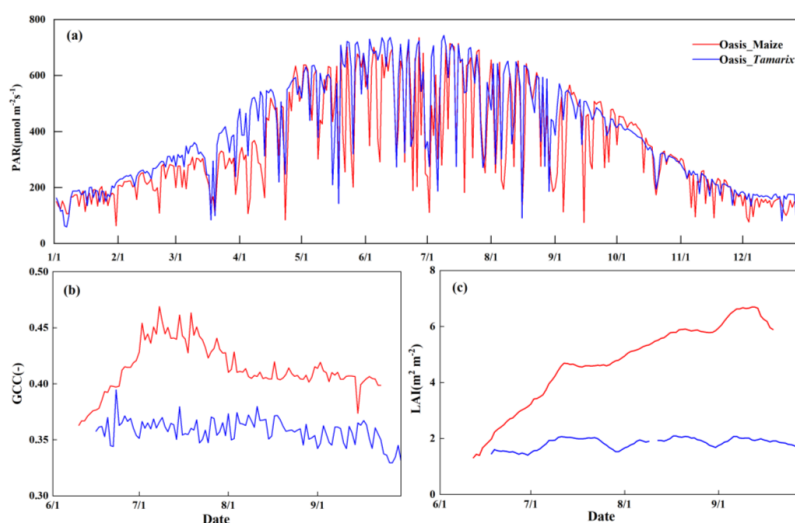
506
507 Fig. 11. Comparison of precipitation and soil moisture profile between desert and oasis
508 (2012-2021, a: oasis in the middle reaches (maize, Daman); b: oasis in the lower reaches
509 (*Tamarix*, Sidaoqiao); c: desert in middle reaches (Bajitan Gobi); d: desert in lower
510 reaches (desert))

511 4.3 Vegetation and soil parameters

512 The vegetation parameters include photosynthetically active radiation (PAR), leaf
513 area index (LAI), phenology, sun-induced chlorophyll fluorescence (SIF), etc. The PAR,
514 the amount of light available for photosynthesis, is observed at stations with vegetation



515 cover, and it can be used as the source of energy for photosynthesis by green plants.
516 The PAR observations showed similar seasonal variations in typical oasis ecosystems
517 in the middle and lower reaches, with a maximum daily PAR of approximately 750
518 $\mu\text{mol m}^{-2} \text{s}^{-1}$ (Fig. 14a). Vegetation parameters, such as LAI and phenology, were also
519 observed in the middle and lower reaches. LAI in the middle reaches (maize) increased
520 gradually with crop growth, and it was larger than that in the lower reaches (*Tamarix*),
521 which showed little change in this shrub surface (Fig. 14b). The phenological camera
522 was installed at each station except the desert to acquire the phenology. The greenness
523 index of the green chromatic coordinate (GCC) was derived to capture the key
524 phenological phase of the plant, such as the SOS (start of season), POP (position of
525 peak value), and EOS (end of season) (Fig. 14c).



526
527 Fig. 12. Variations in vegetation parameters in the middle and lower reaches of the oasis
528 (a, b, c are PAR, LAI and GCC in the artificial and natural oases, respectively, in 2018)

529 Soil samples were collected at each station in the middle and lower reaches in 2012



530 and 2020. These soil samples were analyzed in the laboratory, and parameters such as
 531 soil texture, porosity, bulk density, saturated hydraulic conductivity, and soil organic
 532 matter content were obtained. Some soil parameters at typical stations are shown in
 533 Table 3. Silty soil is dominant in the oasis, and sand is dominant in the desert. The
 534 porosity and bulk density showed no significant difference. The saturated hydraulic
 535 conductivity and soil organic matter at the typical stations are also given in Table 3.

536 Table 3 Soil parameter measurements at typical stations in 2020

	Station	Soil texture	Soil properties
Middle reaches	Daman (Oasis)	Clay: 6%	Porosity: 47.1 %; Bulk density: 1.46 g/cm ³ ; Saturated hydraulic conductivity: 0.177 mm/min; Saturated water capacity: 64.10 %; PH: 8.48; NH ₄ ⁺ -N: 0.83 mg/kg; NO ₃ ⁻ -N: 15.90 mg/kg; Soil carbon content: 1.85 %; Soil organic carbon content: 0.72 %; Soil nitrogen content: 0.027%
		Silt: 69%	
		Sand: 25%	
Lower reaches	Huaizhaizi (Desert)	Clay: 1%	Porosity: 38.0 %; Bulk density: 1.49 g/cm ³ ; Saturated hydraulic conductivity: 4.93 mm/min; Saturated water capacity: 22.21 %; PH: 8.27; NH ₄ ⁺ -N: 0.77 mg/kg; NO ₃ ⁻ -N: 29.70 mg/kg; Soil carbon content: 1.83 %; Soil organic carbon content: 0.33 %; Soil nitrogen content: 0.026%
		Silt: 19%	
		Sand: 80%	
Lower reaches	Sidaoqiao (Oasis)	Clay: 21%	Porosity: 45.8 %; Bulk density: 1.47 g/cm ³ ; PH: 8.80; NH ₄ ⁺ -N: 1.02 mg/kg; NO ₃ ⁻ -N: 5.23 mg/kg; Soil carbon content: 2.02 %; Soil organic carbon content: 0.70 %; Soil nitrogen content: 0.070%
		Silt: 69%	
		Sand: 10%	
Lower reaches	Desert around terminal lake (Desert)	Clay: 9%	Porosity: 44.4 %; Bulk density: 1.49 g/cm ³ ; PH: 8.62; NH ₄ ⁺ -N: 0.26 mg/kg; NO ₃ ⁻ -N: 5.74 mg/kg; Soil carbon content: 1.42 %; Soil organic carbon content: 0.38 %; Soil nitrogen content: 0.039%
		Silt: 7%	
		Sand: 84%	

537 **5. Data availability**

538 The dataset of energy, water vapor and carbon exchange observations in oasis-desert
 539 areas reported in this study, including energy, water vapor and carbon fluxes,
 540 hydrometeorological data, and vegetation and soil parameters, are available and can be
 541 downloaded freely at the National Tibetan Plateau Data Center
 542 (<https://doi.org/10.11888/Terre.tpdc.300441>, Liu et al., 2023). A specific directory for
 543 each observation station was designated with data classified into three categories,



544 namely, energy, water vapor and carbon fluxes, hydrometeorological data, and
545 vegetation and soil parameter data. Short descriptions were also provided for each
546 dataset. The Beijing standard time was used in all the data files (UTC+8).

547 **6. Conclusions**

548 The typical land covers in the middle and lower reaches over the HRB are oases and
549 deserts characterized by fragile environments. Oasisization and desertification are two
550 opposing processes in arid and semiarid regions with scarce water resources. To combat
551 desertification around oases and maintain the sustainable development of oases, a land
552 surface process integrated observatory network was established in the oasis-desert area
553 in the middle and lower reaches of the HRB. Eleven stations (7 in oasis, 4 in desert)
554 have been established in these regions since 2012 to monitor the energy, water vapor
555 and carbon exchange between land and atmosphere over oasis and desert areas, and a
556 long-term and high-quality oasis and desert dataset of energy, water vapor and carbon
557 fluxes and auxiliary parameters was produced. This study shows the achievements of
558 11 stations over 10 continuous years of observations, including energy, water vapor and
559 carbon fluxes, hydrometeorology, vegetation and soil parameter data. These data can
560 be used in the analysis of the water-heat-carbon process and its influence mechanism
561 (Wang et al., 2019; Xu et al., 2020; Bai et al., 2021; Wu et al., 2023), calibration and
562 validation of remote sensing products (Ma et al., 2018; Song et al., 2018; Li et al., 2021;
563 Zhang et al., 2022), and simulations of energy, water vapor and carbon exchange (Li et
564 al., 2017b; Liu et al., 2020; He et al., 2022; Zhou et al., 2022). We confirm that the 10-
565 year long-term dataset presented in this study is of high quality with few missing data



566 and believe that the datasets will support ecological security and sustainable
567 development in oasis-desert areas. Most of the stations are ongoing observations, which
568 can play a greater role in such ecologically fragile areas and provide a reference for
569 other similar oasis-desert areas along the Silk Road.

570

571 **Acknowledgement**

572 This work was supported by the Strategic Priority Research Program of the Chinese
573 Academy of Sciences (Grant no. XDA20100101), the National Natural Science
574 Foundation of China (42171461).

575

576 **References:**

577 Bai, Y., Liu, Y. L., Kueppers, L. M., Feng, X., Yu, K. L., Yang, X. F., Li, X. Y., and
578 Huang, J. P.: The coupled effect of soil and atmospheric constraints on stress-
579 responses of desert riparian species, *Agr. Forest Meteorol.*, 311, 108701,
580 <https://doi.org/10.1016/j.agrformet.2021.108701>, 2021.

581 Cheng, G. D., Xiao, D. N., and Wang, G. X.: On the characteristics and building of
582 landscape ecology in arid area, *Adv. Geosci.*, 14 (1), 11–15, 1999. (in Chinese with
583 English abstract).

584 Cheng, G. D., Li, X., Zhao, W., Xu, Z., Feng, Q., Xiao, S. and Xiao, H.: Integrated study
585 of the water-ecosystem-economy in the Heihe River Basin, *Natl. Sci. Rev.*, 1(3), 413-
586 428, <https://doi.org/10.1093/nsr/nwu017>, 2014.

587 Chu, P. C., Lu, S., and Chen, Y.: A numerical modeling study on desert oasis self-
588 supporting mechanisms, *J. Hydrol.*, 312, 256-276,



- 589 <https://doi.org/10.1016/j.jhydrol.2005.02.043>, 2005.
- 590 Crétaux, J. F., Calmant, S., Romanovski, V., Shabunin, A., Lyard, F., Bergé-Nguyen,
591 M., Cazenave, A., Hernandez, F., and Perosanz, F.: An absolute calibration site for
592 radar altimeters in the continental domain: Lake Issykkul in the central Asia, *J.*
593 *Geodesy*, 83(8), 723-735, <http://doi.org/10.1007/s00190-008-0289-7>, 2009.
- 594 Dregne, H. E.: Global status of desertification, *Annals of Arid Zone*, 30, 179–185,
595 <https://epubs.icar.org.in/index.php/AAZ/article/view/64733>, 1991.
- 596 Georgescu, M., Moustauoui, M., Mahalov, A., and Dudhia, J.: An alternative explanation
597 of the semiarid urban area “oasis effect”, *J. Geophys. Res.-Atmos.*, 116, D24113,
598 <https://doi.org/10.1029/2011JD016720>, 2011.
- 599 He, X. L., Liu, S. M., Xu, T. R., Yu, K. L., Gentine, P., Zhang, Z., Xu, Z. W., Jiao, D.
600 D., and Wu, D. X.: Improving predictions of evapotranspiration by integrating multi-
601 source observations and land surface model, *Agr. Water Manage.*, 272, 107827,
602 <https://doi.org/10.1016/j.agwat.2022.107827>, 2022.
- 603 Hommeltenberg, J., Mauder, M., Drosler, M., Heidbach, K., Werle, P., and Schmid, H.
604 P.: Ecosystem scale methane fluxes in a natural temperate bog-pine forest in
605 southern Germany, *Agric. For. Meteorol.*, 198–199, 273–284,
606 <https://doi.org/10.1016/j.agrformet.2014.08.017>, 2014.
- 607 Huang, J. P., Yu, H. P., Guan, X. D., Wang, G. Y., and Guo, R. X.: Accelerated dryland
608 expansion under climate change, *Nature Clim. Change*, 6, 166-171,
609 <https://doi.org/10.1038/nclimate2837>, 2016.
- 610 Liebenthal, C., Huwe, B., and Foken, T.: Sensitivity analysis for two ground heat flux



611 calculation approaches, *Agric. For. Meteorol.*, 132(3–4), 253–262,
612 <https://doi.org/10.1016/j.agrformet.2005.08.00>, 2005.

613 Li, M. S., Zhou, J., Peng, Z. X., Liu, S. M., Göttsche, F. M., Zhang, X. D., and Song, L.
614 S.: Component radiative temperatures over sparsely vegetated surfaces and their
615 potential for upscaling land surface temperature, *Agric. For. Meteorol.*, 276–277,
616 107600, <https://doi.org/10.1016/j.agrformet.2019.05.031>, 2019.

617 Li, X., Li, X. W., Li, Z. Y., Ma, M. G., Wang, J., Xiao, Q., Liu, Q., Che, T., Chen, E. X.,
618 Yan, G. J., Hu, Z. Y., Zhang, L. X., Chu, R. Z., Su, P. X., Liu, Q. H., Liu, S. M.,
619 Wang, J. D., Niu, Z., Chen, Y., Jin, R., Wang, W. Z., Ran, Y. H., and Xin, X.:
620 Watershed Allied Telemetry Experimental Research, *J. Geophys. Res.-Atmos.*,
621 114, D22103, <https://doi.org/10.1029/2008JD011590>, 2009.

622 Li, X., Cheng, G. D., Liu, S. M., Xiao, Q., Ma, M. G., Jin, R., Che, T., Liu, Q. H., Wang,
623 W. Z., Qi, Y., Wen, J. G., Li, H. Y., Zhu, G. F., Guo, J. W., Ran, Y. H., Wang, S. G.,
624 Zhu, Z. L., Zhou, J., Hu, X. L., and Xu, Z. W.: Heihe Watershed Allied Telemetry
625 Experimental Research (HiWATER): Scientific Objectives and Experimental
626 Design, *B. Am. Meteorol. Soc.*, 94, 1145–1160, [https://doi.org/10.1175/BAMS-](https://doi.org/10.1175/BAMS-D-12-00154.1)
627 [D-12-00154.1](https://doi.org/10.1175/BAMS-D-12-00154.1), 2013.

628 Li, X., Yang, K., and Zhou, Y.: Progress in the study of oasis-desert interactions, *Agric.*
629 *For. Meteorol.*, 230, 1–7, <https://doi.org/10.1016/j.agrformet.2016.08.022>, 2016.

630 Li, X., Liu, S. M., Xiao, Q., Ma, M. G., Jin, R., Che, T., Wang, W. Z., Hu, X. L., Xu, Z.
631 W., Wen, J. G., and Wang, L. X.: A multiscale dataset for understanding complex
632 eco-hydrological processes in a heterogeneous oasis system, *Sci. Data*, 4, 170083,



- 633 <https://doi.org/10.1038/sdata.2017.83>, 2017a.
- 634 Li, X., Zheng, Y., Sun, Z., Tian, Y., Zheng, C. M., Liu, J., Liu, S. M., and Xu, Z. W.: An
635 integrated ecohydrological modeling approach to exploring the dynamic
636 interaction between groundwater and phreatophytes, *Ecol. Model.*, 356, 127-140,
637 <https://doi.org/10.1016/j.ecolmodel.2017.04.017>, 2017b.
- 638 Li, X., Liu, S. M., Li, H. X., Ma, Y. F., Wang, J. H., Zhang, Y., Xu, Z. W., Xu, T. R.,
639 Song, L. S., Yang, X. F., Lu, Z., Wang, Z. Y., and Guo, Z. X.: Intercomparison of
640 six upscaling evapotranspiration methods: from site to the satellite pixel, *J.*
641 *Geophys. Res.-Atmos.*, 123, 6777-6803, <https://doi.org/10.1029/2018JD028422>,
642 2018.
- 643 Li, X., Liu, S. M., Yang, X. F., Ma, Y. F., He, X. L., Xu, Z. W., Xu, T. R., Song, L. S.,
644 Zhang, Y., Hu, X., Qu, Q., and Zhang, X. D.: Upscaling evapotranspiration from a
645 single-site to satellite pixel scale, *Remote Sen.*, 13, 4072,
646 <https://doi.org/10.3390/rs13204072>, 2021.
- 647 Liu, R., Sogachev, A., Yang, X. F., Liu, S. M., Xu, T. R., and Zhang, J. J.: Investigating
648 microclimate effects in an oasis-desert interaction zone, *Agric. For. Meteorol.*, 290,
649 107992, <https://doi.org/10.1016/j.agrformet.2020.107992>, 2020.
- 650 Liu, S. M., Xu, Z. W., Wang, W. Z., Bai, J., Jia, Z. Z., Zhu, M. J., and Wang, J. M.: A
651 comparison of eddy-covariance and large aperture scintillometer measurements
652 with respect to the energy balance closure problem. *Hydrol. Earth Syst. Sci.*, 15(4),
653 1291-1306, <https://doi.org/10.5194/hess-15-1291-2011>, 2011.
- 654 Liu, S. M., Xu, Z. W., Song, L. S., Zhao, Q. Y., Ge, Y., Xu, T. R., Ma, Y. F., Zhu, Z. L.,



- 655 Jia, Z. Z., and Zhang, F.: Upscaling evapotranspiration measurements from multi-
656 site to the satellite pixel scale over heterogeneous land surfaces, *Agric. For.*
657 *Meteorol.*, 230-231, 97-113, <https://doi.org/10.1016/j.agrformet.2016.04.008>,
658 2016.
- 659 Liu, S. M., Li, X., Xu, Z. W., Che, T., Xiao, Q., Ma, M. G., Liu, Q. H., Jin, R., Guo, J.
660 W., Wang, L. X., Wang, W. Z., Qi, Y., Li, H. Y., Xu, T. R., Ran, Y. H., Hu, X. L.,
661 Shi, S. J., Zhu, Z. L., Tan, J. L., Zhang, Y., and Ren, Z.G.: The Heihe Integrated
662 Observatory Network: A basin-scale land surface processes observatory in China,
663 *Vadose Zone J.*, 17, 180072, <https://doi.org/10.2136/vzj2018.04.0072>, 2018.
- 664 Liu, S., Xu, Z., Che, T., Li, X., Xu, T., Ren, Z., Zhang, Y., Tan, J., Song, L., Zhou, J.,
665 Zhu, Z., Yang, X., Liu, R., and Ma, Y.: Energy, water vapor and carbon exchange
666 observations in oasis-desert areas of Heihe river basin (2012-2021), National
667 Tibetan Plateau/Third Pole Environment Data Center,
668 <https://doi.org/10.11888/Terre.tpdc.300441>, 2023.
- 669 Ma, Y. F., Liu, S. M., Song, L. S., Xu, Z. W., Liu, Y. L., Xu, T. R., and Zhu, Z. L.:
670 Estimation of daily evapotranspiration and irrigation water efficiency at a Landsat-
671 like scale for an arid irrigation area using multi-source remote sensing data, *Remote*
672 *sens. environ.*, 216, 715-734, <https://doi.org/10.1016/j.rse.2018.07.019>, 2018.
- 673 Mao, D., Wang, Z., Wu, B., Zeng, Y., Luo, L., and Zhang, B: Land degradation and
674 restoration in the arid and semiarid zones of China: Quantified evidence and
675 implications from satellites. *Land degrad. Dev.*, 29(11), 3841-3851,
676 <https://doi.org/10.1002/ldr.3135>, 2018.



- 677 Meng, X., Lv, S., Zhang, T., Guo, J., Gao, Y., Bao, Y., Wen, L., Luo, S., and Liu, Y.:
678 Numerical simulations of the atmospheric and land conditions over the jinta oasis in
679 northwestern China with satellite-derived land surface parameters, *J. Geophys. Res.-*
680 *Atmos.*, 114, 605-617, <https://doi.org/10.1029/2008JD010360>, 2009.
- 681 Potchter, O., Goldman, D., Kadish, D., and Iluz, D.: The oasis effect in an extremely
682 hot and arid climate: The case of southern Israel, *J. Arid Environ.*, 72, 1721-1733,
683 <https://doi.org/10.1016/j.jaridenv.2008.03.004>, 2008.
- 684 Qu, Y. H., Zhu, Y. Q., Han, W. C., Wang, J. D., and Ma, M. G: Crop leaf area index
685 observations with a wireless sensor network and its potential for validating remote
686 sensing products, *IEEE J-STARS.*, 7(2), 431-444,
687 <https://doi.org/10.1109/JSTARS.2013.2289931>, 2014.
- 688 Scanlon, B. R., Keese, K. E., Flint, A. L., Flint, L. E., Gaye, C. B., Edmunds, W. M.,
689 and Simmers, I.: Global synthesis of groundwater recharge in semiarid and arid
690 regions, *Hydrol. Process*, 20 (15), 3335–3370, <https://doi.org/10.1002/hyp.6335>,
691 2006.
- 692 Stone, K. B.: Burke-Litwin organizational assessment survey: reliability and validity,
693 *Organization development journal*, 33(2), 33-50, 2015.
- 694 Stanev, E., Staneva, J., Bullister, J., and Murray, J.: Ventilation of the black sea
695 pycnocline. Parameterization of convection, numerical simulations and validations
696 against observed chlorofluorocarbon data, *Deep sea research part I: Oceanographic*
697 *research papers*, 51 (12), 2137-2169, <https://doi.org/10.1016/j.dsr.2004.07.018>, 2004.
- 698 Song, L.S., Liu, S.M., Kustas, W.P., Nieto, H., Sun, L., Xu, Z.W., Skaggs, T.H., Yang,



- 699 Y., Ma, M.G., Xu, T.R., Tang, X.G., and Li, Q.P.: Monitoring and validating spatially
700 and temporally continuous daily evaporation and transpiration at river basin scale,
701 *Remote sens. environ.*, 219, 72-88, <https://doi.org/10.1016/j.rse.2018.10.002>, 2018.
- 702 Taha, H., Akbari, H., and Rosenfeld, A.: Heat island and oasis effects of vegetative
703 canopies, *Theor. Appl. Climatol.*, 44, 123-138, <https://doi.org/10.1007/BF00867999>,
704 1991.
- 705 Tagesson, T., Fensholt, R., Cappelaere, B., Mougin, E., Horion, S., Kergoat, L., Nieto,
706 H., Mbow, C., Ehammer, A., Demarty, J., and Ardö, J.: Spatiotemporal variability in
707 carbon exchange fluxes across the Sahel, *Agric. For. Meteorol.*, 226-227, 108-118,
708 <https://doi.org/10.1016/j.agrformet.2016.05.013>, 2016.
- 709 Wang, J. M., and Mitsuta, Y.: Evaporation from the desert: some preliminary results of
710 HEIFE, *Boundary Layer Meteorology*, 59, 413-418,
711 <https://doi.org/10.1007/BF0221546>, 1992.
- 712 Wang, G. X., and Cheng, G. D.: Water resource development and its influence on the
713 environment in arid areas of China-the case of the Hei River basin, *J. Arid Environ.*,
714 43, 121–131, <https://doi.org/10.1006/jare.1999.0563>, 1999.
- 715 Wang, H. B., Li, X., Xiao, J. F., Ma, M. G., Tan, J. L., Wang, X. F., and Geng, L. Y.:
716 Carbon fluxes across alpine, oasis, and desert ecosystems in northwestern China: The
717 importance of water availability, *Sci. total environ.*, 697, 133978,
718 <https://doi.org/10.1016/j.scitotenv.2019.133978>, 2019.
- 719 Wen, X., Lv, S., and Jin, J.: Integrating remote sensing data with WRF for improved
720 simulations of oasis effects on local weather processes over an arid region in



- 721 northwestern China, J. Hydrometeorol., 13(2), 573-587,
722 <https://doi.org/10.1175/JHM-D-10-05001.1>, 2012.
- 723 Wu, D. X., Liu, S. M., Wu, X. C., Xu, T. R., Xu, Z. W., He, X. L., and Shi, H. Y.:
724 Evaluation of the intrinsic temperature sensitivity of ecosystem respiration in typical
725 ecosystems of an endorheic river basin, *Agric. For. Meteorol.*, 333, 109393,
726 <https://doi.org/10.1016/j.agrformet.2023.109393>, 2023.
- 727 Xu, Z. W., Liu, S. M., Li, X., Shi, S. J., Wang, J. M., Zhu, Z. L., Xu, T. R., Wang, W.
728 Z., and Ma, M. G.: Intercomparison of surface energy flux measurement systems
729 used during the HiWATER-MUSOEXE, *J. Geophys. Res.-Atmos.*, 118, 13140-
730 13157, <https://doi.org/10.1002/2013JD020260>, 2013.
- 731 Xu, Z. W., Liu, S. M., Zhu, Z. L., Zhou, J., Shi, W. J., Xu, T. R., Yang, X. F., Zhang, Y.,
732 and He, X.L.: Exploring evapotranspiration changes in a typical endorheic basin
733 through the integrated observatory network, *Agric. For. Meteorol.*, 290, 108010,
734 <https://doi.org/10.1016/j.agrformet.2020.108010>, 2020.
- 735 Xue, J., Gui, D., Lei, J., Sun, H., Zeng, F., Mao, D., Zhang, Z., Jin, Q., and Liu, Y.:
736 Oasis microclimate effects under different weather events in arid or hyper arid
737 regions: A case analysis in southern Taklimakan desert and implication for
738 maintaining oasis sustainability, *Theor. Appl. Climatol.*, 137, 89-101,
739 <https://doi.org/10.1007/s00704-018-2567-5>, 2019.
- 740 Zhang, Y. Y., and Zhao, W. Z.: Vegetation and soil property response of short-
741 timefencing in temperate desert of the Hexi Corridor northwestern China, *Catena*,
742 133, 43–51, <https://doi.org/10.1016/j.catena.2015.04.019>, 2015.



- 743 Zhang, X. Y., Arimoto, R., Zhu, G. H., Chen, T., and Zhang, G. Y.: Concentration, size-
744 distribution and deposition of mineral aerosol over Chinese desert regions, *Tellus B:*
745 *Chemical and Physical Meteorology*, 50(4), 317-330,
746 <https://doi.org/10.3402/tellusb.v50i4.16131>, 2016a.
- 747 Zhang, Q., Sun, R., Jiang, G.Q., Xu, Z. W., and Liu, S. M.: Carbon and energy flux
748 from a *Phragmites australis* wetland in Zhangye oasis-desert area, China, *Agric. For.*
749 *Meteorol.*, 230-231, 45-57, <https://doi.org/10.1016/j.agrformet.2016.02.019>, 2016b.
- 750 Zhang, Y., Zhao, W., He, J., and Fu, L.: Soil susceptibility to macropore flow across a
751 desert-oasis ecotone of the Hexi Corridor, Northwest China, *Water Resour. Res.*, 54,
752 1281–1294, <https://doi.org/10.1002/2017WR021462>, 2018.
- 753 Zhang, Z., Poulter, B., Knox, S., Stavert, A., McNicol, G., Fluet-Chouinard, E.,
754 Feinberg, A., Zhao, Y., Bousquet, P., Canadell, J., Ganesan, A., Hugelius, G., Jackson,
755 R., Patra, P., Saunio, M., Höglund-Isaksson, L., Huang, C., Chatterjee, A., and Li,
756 X.: Anthropogenic emission is the main contributor to the rise of atmospheric
757 methane during 1993–2017, *Natl. Sci. Rev.*, 9(5), nwab200,
758 <https://doi.org/10.1093/nsr/nwab200>, 2022.
- 759 Zhang, Y., Liu, S. M., Song, L. S., Li, X., Jia, Z. Z., Xu, T. R., Xu, Z. W., Ma, Y. F.,
760 Zhou, J., Yang, X. F., He, X. L., Yao, Y. J., and Hu, G. C.: Integrated Validation of
761 Coarse Remotely Sensed Evapotranspiration Products over Heterogeneous Land
762 Surfaces, *Remote Sens.*, 14, 3467, <https://doi.org/10.3390/rs14143467>, 2022.
- 763 Zhao, R., Chen, Y., Shi, P., Zhang, L., Pan, J., and Zhao, H.: Land use and land cover
764 change and driving mechanism in the arid inland river basin: a case study of Tarim



765 River, Xinjiang, China, *Environ. Earth sci.*, 68(2), 591-604, <https://doi>
766 [10.1007/s12665-012-1763-3](https://doi.org/10.1007/s12665-012-1763-3), 2013.

767 Zheng, C., Liu, S. M., Song, L. S., Xu, Z. W., Guo, J. X., Ma, Y. F., Ju, Q., and Wang,
768 J. M.: Comparison of sensible and latent heat fluxes from optical-microwave
769 scintillometers and eddy covariance systems with respect to surface energy balance
770 closure, *Agric. For. Meteorol.*, 331, 109345,
771 <https://doi.org/10.1016/j.agrformet.2023.109345>, 2023.

772 Zhou, Y., Liao, W., and Li, X.: The contributions of individual factors to the oasis cold
773 island effect intensity in the Heihe River Basin, *Agric. For. Meteorol.*, 312, 108706,
774 <https://doi.org/10.1016/j.agrformet.2021.108706>, 2022.